

# Sensitivity of rocky planet structures to the equation of state

Damian C. Swift

*PLS-CMMD, Lawrence Livermore National Laboratory,  
7000 East Avenue, Livermore, California 94550, USA*

(Dated: June 10, 2009 – LLNL-TR-414058)

Structures were calculated for Mercury, Venus, Earth, the Moon, and Mars, using a core-mantle model and adjusting the core radius to reproduce the observed mass and diameter of each body. Structures were calculated using Fe and basalt equations of state of different degrees of sophistication for the core and mantle. The choice of equation of state had a significant effect on the inferred structure. For each structure, the moment of inertia ratio was calculated and compared with observed values. Linear Grüneisen equations of state fitted to limited portions of shock data reproduced the observed moments of inertia significantly better than did more detailed equations of state incorporating phase transitions, presumably reflecting the actual compositions of the bodies. The linear Grüneisen equations of state and corresponding structures seem however to be a reasonable starting point for comparative simulations of large-scale astrophysical impacts.

## I. INTRODUCTION

The pressure-temperature-compression equation of state (EOS) of condensed matter is vital in understanding planetary structures, and the response of astrophysical bodies to impacts. Even for Earth, it is necessary to infer the internal structure of the planet from limited data. The situation is much more difficult for other bodies, where seismic data is at best extremely limited and more usually absent.

For planetary structures, we are usually interested in pressures from zero to a few hundred gigapascals. In this range, EOS were originally deduced empirically from shock wave measurements [1]. Shock experiments typically explore states along the principal Hugoniot of a material, which may be significantly hotter than the corresponding compression or pressure occurring in a self-gravitating body, and corrections are made to estimate the pressure away from the Hugoniot [1]. More recently, mechanical presses such as diamond anvil cells have provided a source for isothermal compression in this regime, although the pressure calibration is made with respect to shock measurements on reference materials [2]. Samples may also be heated within presses, allowing a wide range of states to be explored. In parallel with the evolution of experimental methods, theoretical techniques have been developed to predict the EOS from first principles, typically with an *a priori* accuracy of a few percent in mass density, and better if adjusted to reproduce the STP state [3]. Theoretical EOS are particularly useful as thermodynamically complete states can be calculated for arbitrary loading conditions that may be experimentally difficult either to induce or to measure. Theoretical EOS can also be constructed fairly readily for different material compositions [4]. The prediction of phase diagrams is however typically less certain than the EOS for a single, known phase.

The strength, failure, and plastic flow behaviors of materials are also important in planetary physics. The effects of strength must be taken into account when deducing the EOS from dynamic loading measurements, as

these are at high strain rates and non-hydrostatic conditions in contrast to the quasistatic conditions prevailing within self-gravitating bodies. Conversely, these properties are important for understanding dynamical processes including the formation of the body, the effect of impacts, cooling, volcanism, mantle convection, and plate tectonics. These constitutive properties are very challenging to predict theoretically, and models rely heavily on experimental measurements. Recent studies have demonstrated the importance of strength in the heating induced by shocks and other dynamic loading [5]. Strength and flow stress can also change greatly with pressure and temperature. Recent advances in the measurement and modeling of plastic flow under extreme conditions has implications for astrophysical impacts, such as the interpretation of previous simulation studies using simpler material models. An example is the widely-quoted study that a liquid interior allow impact energy to be transported more efficiently to the antipode of an impact than would solid components [6]. This conclusion relies strongly on the assumptions used for material strength. If the flow stress increases sufficiently with compression, solid components can transport compression waves more efficiently than can liquids.

We are constructing theoretical EOS for planetary materials of different composition, for use in simulations of astrophysical impacts, focusing on systematic differences in the shape and location of impact-produced structures between the rocky bodies. As a baseline for trial simulations, we report here the construction of structure models for the rocky planets using existing EOS of different sophistication. There is significant uncertainty over the composition and temperature profile of all planetary bodies; here we use EOS for representative substances rather than for the current best estimates of composition, because a wider variety of EOS of different degrees of sophistication exist for our chosen materials. We optimize a single structure parameter – the core radius – for each combination of EOS. This approach is different from the commonly-used solution of the Emden equation [7, 8] where the compressibility of the planetary material

is assumed to vary linearly with pressure, and the parameters in this relation – i.e., the material properties – are deduced from the observable properties of the planet.

## II. ISOSTATIC STRUCTURES

Consider a spherical body comprising compressible material, of mass density  $\rho(r)$ . Knowing or assuming in addition the distribution of composition and temperature,  $\rho(r)$  implies a pressure distribution  $p(r)$ . The condition for isostatic equilibrium is that the stress induced by pressure variations is balanced by the gravitational acceleration  $g(r)$  and centripetal force:

$$\text{grad } p(r) = \omega^2 - \rho(r)g(r) \quad (1)$$

where  $\omega$  is the angular speed.

For Newtonian gravitation, by Gauss' theorem,  $g(r)$  can be expressed in terms of the mass enclosed within a given radius  $m(r)$ :

$$g(r) = \frac{Gm(r)}{r^2} \quad (2)$$

so

$$\frac{dg(r)}{dr} = G \left( \frac{1}{r^2} \frac{dm(r)}{dr} - 2 \frac{m(r)}{r^3} \right). \quad (3)$$

$m(r)$  can be calculated simply from the distribution of mass density,

$$m(r) = 4\pi \int_0^r r'^2 \rho(r') dr' \quad (4)$$

or

$$\frac{dm(r)}{dr} = 4\pi r^2 \rho(r). \quad (5)$$

In the isostatic equilibrium structure, Eq. 5 can be integrated from either the center or the surface  $r = R$  to obtain the complete structure. In practice, the material state at the center depends on the material models used, so it is more useful to integrate from the surface, where  $p = 0$  and  $\rho$  can be worked out simply for the outermost material.

Usually, the total mass  $M$  and outer radius  $R$  of the body are known fairly well from observation of orbits and size respectively, and the problem is to establish the internal structure. Starting with the assumption of a layered structure, i.e. an ordering of composition, and the  $p(\rho)$  relation for each layer, any unknown parameter in the structure can be fitted to give the desired total mass.

For example, consider a layered structure where the radius of one layer is unknown. For a stable configuration, inner layers have a higher density. Consider integration downward from the surface as above, assuming a trial value for the unknown radius. If too large, the total mass

$M$  will be reached at some  $r > 0$ ; if too small,  $m(0) > 0$ . These two conditions can be used for a solution of this shooting problem by bracketing followed by bisection.

Another remotely observable structural parameter is the moment of inertia  $I$ , which can be inferred from the rate of precession of the rotational pole about the normal to the orbit [9]. In the absence of seismic data,  $I$  is a useful constraint on the structure of the body. The moment of inertia for a sphere is

$$I = \frac{8\pi}{3} \int_0^R \rho(r) r^4 dr, \quad (6)$$

and for self-gravitating bodies is conveniently expressed as the dimensionless moment of inertia ratio,  $I/MR^2$ .

Similar approaches assuming the EOS and deducing isostatic planetary structures have been reported previously. Kerley has calculated structures for Jupiter and Saturn, including rotational flattening, using the theory of figures and very detailed EOS [10]. Seager et al have predicted mass-radius relationships for solid exoplanets, using EOS which are less suited to subsequent impact studies and a different solution approach involving integration outward from the center of the planet [11]. Grasset et al have similarly predicted mass-radius relationships for rocky and icy exoplanets, again using EOS which are less suited to impact studies [12].

## III. COMPRESSIBILITY CURVES FOR DIFFERENT EQUATIONS OF STATE

Two types of EOS were considered: linear Grüneisen EOS using a representative part of the principal shock Hugoniot as reference, and more elaborate EOS constructions incorporating phase transitions and reproducing detailed features of the shock Hugoniot. The shock Hugoniot data used to calibrate the Grüneisen EOS are reliable in the sense of being absolute, mechanical measurements, but require the additional assumption of a thermal correction model to calculate states off the principal Hugoniot, as are required here.

There is considerable uncertainty in the composition of planetary interiors, and detailed EOS are not available for all compositions of interest. In order to calculate structures for all the rocky planets without introducing additional degrees of freedom in the individual compositions, the compositions were taken to be pure Fe in the core, and basalt in the mantle. At zero pressure, basalt typically comprises  $\sim 70\%$  plagioclase (often andesite) and  $\sim 30\%$  olivine, and is thus reasonably representative of the composition thought to occur through the mantle. Further subdivision of layers was not considered; the structure chosen allowed the core radius to be used as a parameter to ensure the correct total mass for each body. Similar structure calculations using detailed EOS for other compositions will be reported separately.

For both Fe and basalt, the shock speed-particle speed relation does not follow a straight line over the full pres-

TABLE I: Linear Grüneisen equation of state parameters.

	Fe	basalt
$\rho_0$ (g/cm <sup>3</sup> )	7.86	2.67
$c_0$ (km/s)	3.635	1.45
$s_1$	1.802	1.97
$\Gamma$	2.604	1.5

sure range of interest. For basalt, a straight line was chosen that reproduced the principal Hugoniot at pressures of a few tens of gigapascals [13], as a representative range for planetary mantles. Similarly, the fit to Fe shock data was for pressures  $\sim 50$ -500 GPa [13]. The more detailed EOS for basalt was a tabulated Grüneisen form using three piecewise linear fits to the principal Hugoniot [14]. The detailed Fe EOS was an equilibrium construction comprising four solid phases and the fluid, with mixed-phase regions [15], and should be much more accurate away from the principal Hugoniot.

In the absence of accurately-known composition profiles, the use of simple EOS is desirable as it allows planetary structures to be optimized via the EOS parameters, though this optimization was not done here. It is much more cumbersome to optimize detailed EOS in this way, particularly when presented in tabular form.

The compression curve used was the principal isentrope. This is a reasonable approach for large, self-gravitating objects. One would expect  $p(\rho)$  to be close to an isentrope on initial formation, as accretion proceeds by multiple small impacts followed by some stratification as dense components sink toward the center of the body. After formation, the decay of radionuclides (and possibly other processes such as tidal deformation and ohmic heating) may supply additional heat, but the surface of the body cools by radiation. In the adiabatic compression of non-porous condensed matter, the thermal contribution to pressure is usually much smaller than the repulsion between atoms, so the difference between the isentrope and the isotherm as extreme limits is small compared with the other uncertainties in planetary structure such as the composition.

Each EOS was used in the form  $p(\rho, e)$ , and integrated numerically starting at STP conditions to obtain  $p(\rho)$  along the principal isentrope. The use of the principal isentrope for each constituent gives a discontinuity in temperature where different layers meet, but the effect on pressure is small compared with the uncertainties in composition and temperature. It would be straightforward, though less efficient, to calculate the isentrope starting at the temperature outside each layer. The isentropes for Fe agreed quite closely up to  $\sim 120$  GPa; at higher pressures, the linear Grüneisen EOS was significantly stiffer. The linear Grüneisen EOS for basalt was much softer than the tabular EOS at low pressures, and much stiffer at high pressures, with a crossover at 100 GPa. (Fig. 1.)

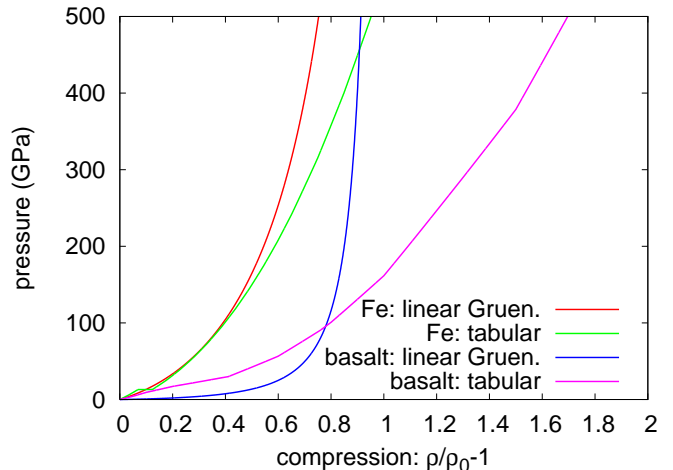


FIG. 1: Comparison between isentropes.

#### IV. PLANETARY STRUCTURES

The planetary structure equation, Eq. 5, was integrated numerically using the 4th order Runge-Kutta algorithm with a constant step size in radius. The effect of rotation was ignored as it depends on latitude; rotation found to be a negligible effect in a trial equatorial integration. The core radius was adjusted to give a density profile consistent with the specified total mass of the body. The step size was chosen such that core radius was converged numerically to 1 km. The resulting moment of inertia ratio was converged to 0.1%, which is better than measured values. The density near the center of the body was very sensitive to small variations in the core radius or any other parameters, often giving unphysical variations for the innermost couple of tens of kilometers. The volume and mass affected were negligible in comparison with the overall body.

Using the linear Grüneisen EOS for core and mantle, the numerical scheme was very robust, and the core radius converged reliably for very wide ranges of the initial bracket. Using the tabular EOS, the initial bracket had to be chosen much more carefully for a physical core radius to be found, because of the increased compressibility of the core. Converged solutions were however found for all the bodies considered and compared with observations of the moment of inertia ratio [16] and the usually-quoted values of the core radius (Table II). We also summarize pressures calculated at the key locations of the mantle-core boundary and the center (Table III) as an indication of the regimes desirable to explore experimentally, for each body.

Given that the EOS used were not for the most likely individual core compositions that have been postulated (Fe-Ni, or Fe-S for Mars), and the planetary structures were simplified, it is interesting to note that the core radius inferred for Earth – the only body for which it can be

TABLE II: Structure parameters for rocky bodies.

body	reference		linear Grüneisen		tabular	
	$r_c$ (km)	$I/MR^2$	$r_c$ (km)	$I/MR^2$	$r_c$ (km)	$I/MR^2$
Mercury	1600	0.33	1740	0.3196	1802	0.3140
Venus	3000	0.33	3014	0.3348	3167	0.3146
Earth	3481	0.33	3361	0.3290	3405	0.3118
Moon	350	0.393	620	0.3647	752	0.3572
Mars	1700±500	0.366	1188	0.3621	1706	0.3316

TABLE III: Key pressures in rocky bodies.

body	linear Grüneisen		tabular	
	center (GPa)	boundary (GPa)	center (GPa)	boundary (GPa)
Mercury	46.5	9.6	47.5	9.6
Venus	318	121	365	120
Earth	390	137	448	143
Moon	8.8	5.0	10.0	4.4
Mars	45.2	27.2	60.0	20.7

estimated using multiple techniques including seismology – is too small by only 2% for the tabular EOS and 3% for the linear Grüneisen. The core radius for the other bodies did not agree very well with the nominal values in the literature, with the exception of Venus, but the difference was commensurate with the uncertainty in radius. The exceptions were Venus, where the agreement was good at 0.5-2% (the linear Grüneisen EOS being the better), and the Moon, where the present calculations were larger by a factor  $\sim 2$ .

For the linear Grüneisen EOS, the moment of inertia ratios were within 3% except for the Moon, for which it was too small by 7%. For the tabular EOS, the ratio was systematically smaller: 4-5% except for the Moon and Mars (9 and 10% respectively). Too small a ratio implies that the body is stiffer than the EOS used in the calculation, in the sense that  $p$  would be greater for a given  $\rho$ . Such an increase in stiffness could reflect a difference in composition rather than too low a stiffness for the material used. Thus the discrepancy for Mars could be attributed to a significant proportion of S, reducing the mass density for a given compression.

The linear Grüneisen EOS gives pressures at the center of the Earth that are within the range of values in the literature (360-390 GPa).

We next compare in more detail the structures predicted for each body by the different EOS.

### A. Mercury

For Mercury, the EOS gave very similar pressure distributions. The core radius from each EOS was similar. The density distribution differed somewhat, particularly in the mantle. The pressure to induce the  $\alpha$ - $\epsilon$  phase change occurred just within the core, and showed up clearly in the density distribution. The gravitational acceleration from each EOS was similar. At the level of detail considered here, the EOS were equivalent. (Figs 2 to 4.)

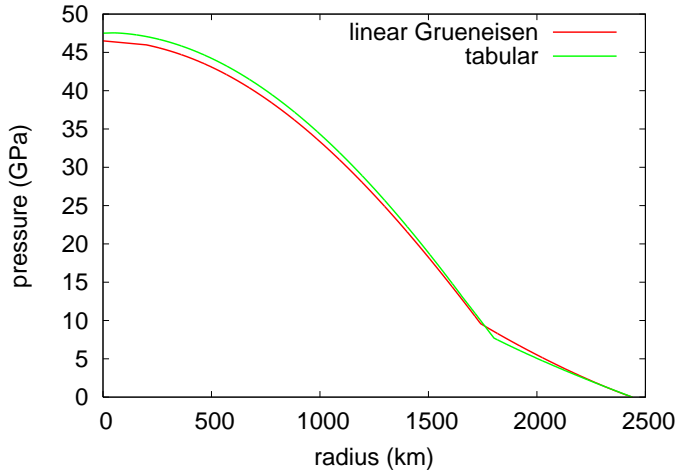


FIG. 2: Radial pressure distribution in Mercury calculated using different equations of state.

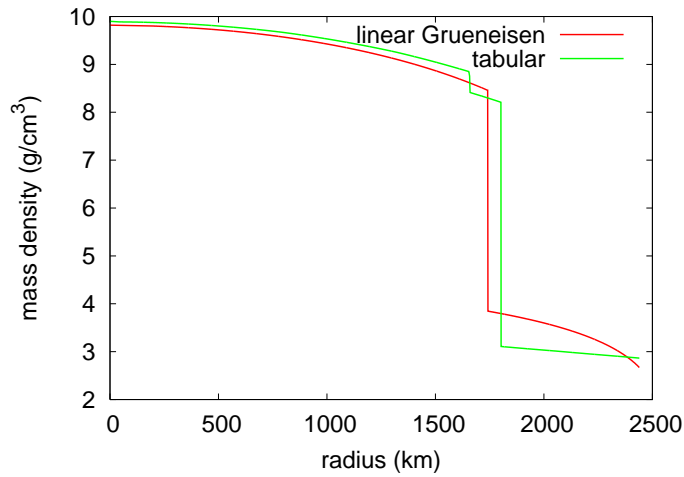


FIG. 3: Radial density distribution in Mercury calculated using different equations of state.

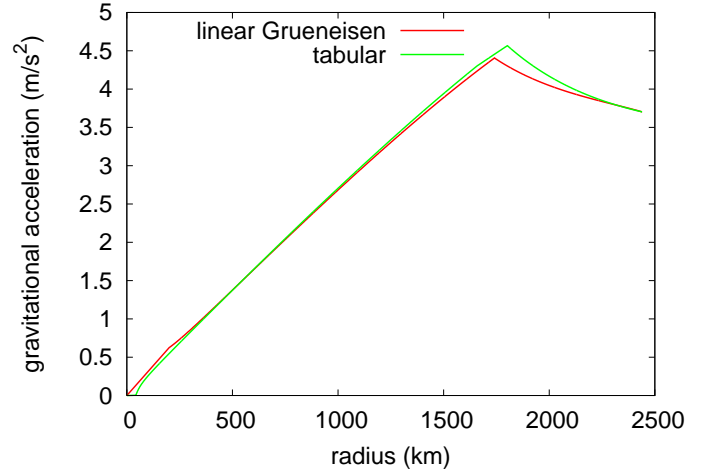


FIG. 4: Radial gravity distribution in Mercury calculated using different equations of state.

### B. Venus

For Venus, the EOS gave very similar pressure distributions in the mantle, and deviated monotonically and significantly in the core. The core radius from each EOS was similar. The density distribution differed somewhat. The core pressure for both EOS was well above the  $\alpha$ - $\epsilon$  phase transition. The gravitational acceleration from each EOS was similar within the core, but differed somewhat in the mantle. At the level of detail considered here, the EOS were not equivalent but conversely not hugely different. (Figs 5 to 7.)

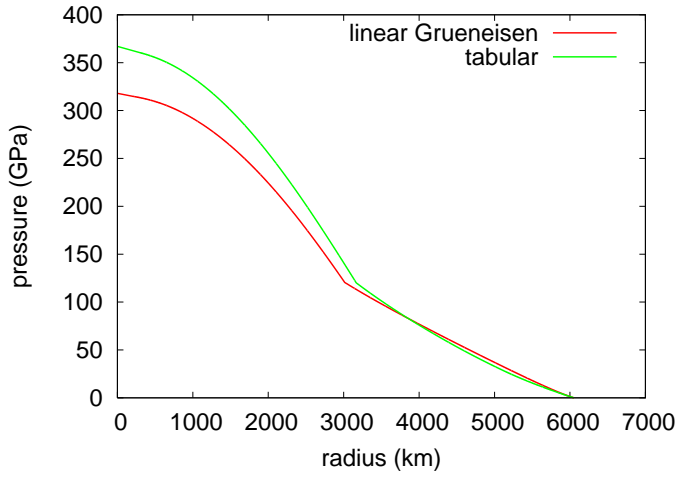


FIG. 5: Radial pressure distribution in Venus calculated using different equations of state.

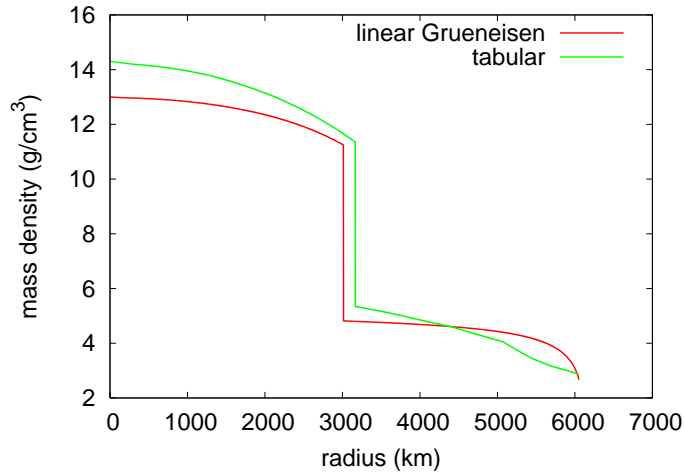


FIG. 6: Radial density distribution in Venus calculated using different equations of state.

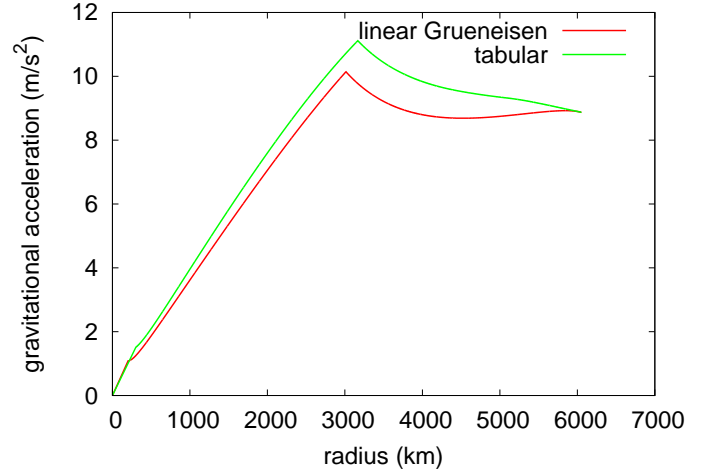


FIG. 7: Radial gravity distribution in Venus calculated using different equations of state.

### C. Earth

The results for Earth were very similar to those for Venus, as one might expect for bodies of similar mass and volume. The EOS gave similar pressure distributions in the mantle, and deviated monotonically and significantly in the core. The core radius from each EOS was very similar. The density distribution differed somewhat. The core pressure for both EOS was well above the  $\alpha$ - $\epsilon$  phase transition. The gravitational acceleration from each EOS differed somewhat over the whole profile (except for the ends, which are constrained to be equal), although the shapes were very similar. At the level of detail considered here, the EOS were not equivalent but not hugely different. (Figs 8 to 10.)

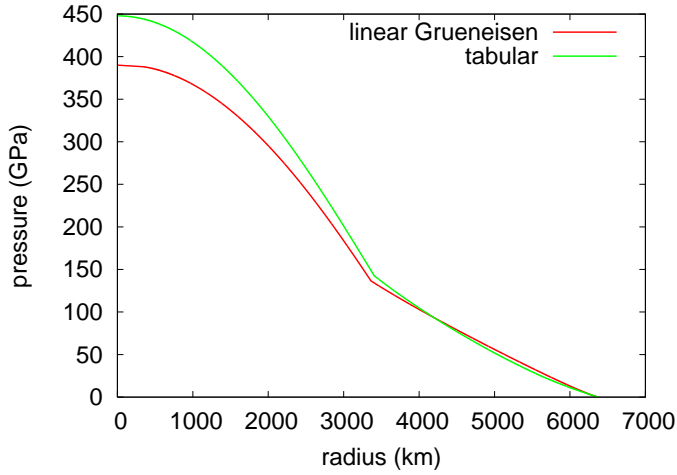


FIG. 8: Radial pressure distribution in Earth calculated using different equations of state.

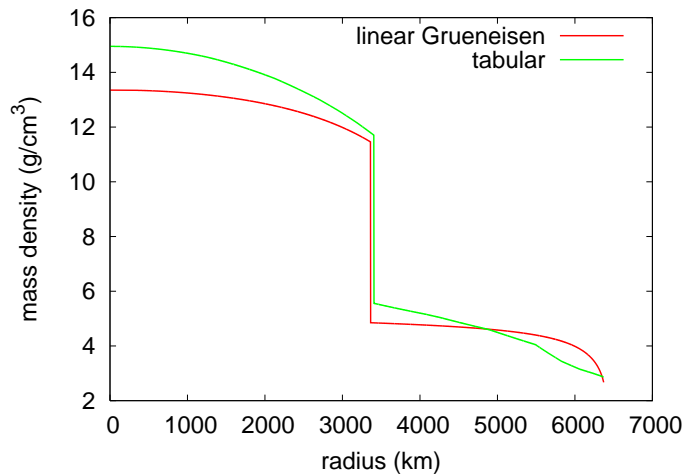


FIG. 9: Radial density distribution in Earth calculated using different equations of state.

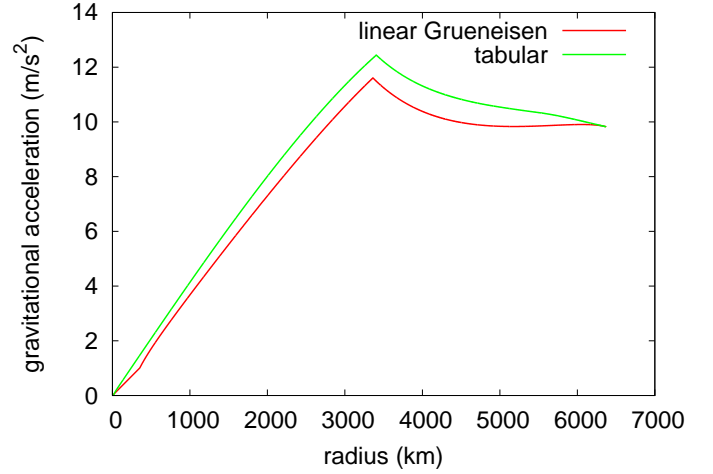


FIG. 10: Radial gravity distribution in Earth calculated using different equations of state.

### D. Moon

For the Moon, the EOS gave very similar pressure distributions in the mantle, and deviated monotonically and significantly in the core. The core radii differed significantly. The density distributions were very similar, particularly in the core, except for the difference in core radius. differed somewhat, particularly in the mantle. The core pressures were all below the  $\alpha$ - $\epsilon$  phase transition. The gravitational acceleration from each EOS was very similar in the core, but deviated substantially where the core radii differed and in the inner mantle. At the level of detail considered here, the EOS were fairly equivalent. (Figs 11 to 13.)

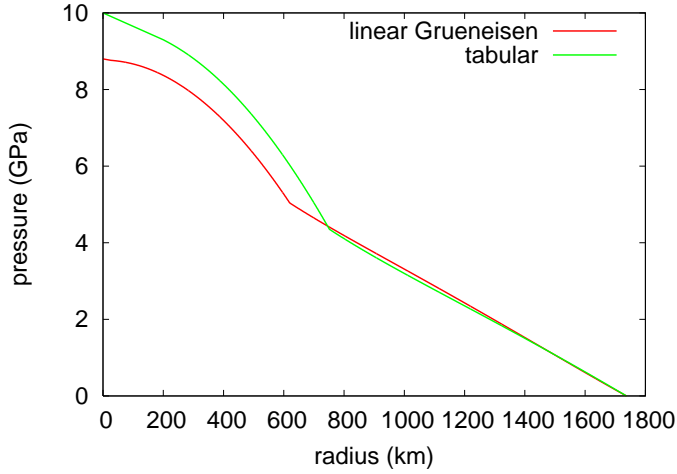


FIG. 11: Radial pressure distribution in the Moon calculated using different equations of state.

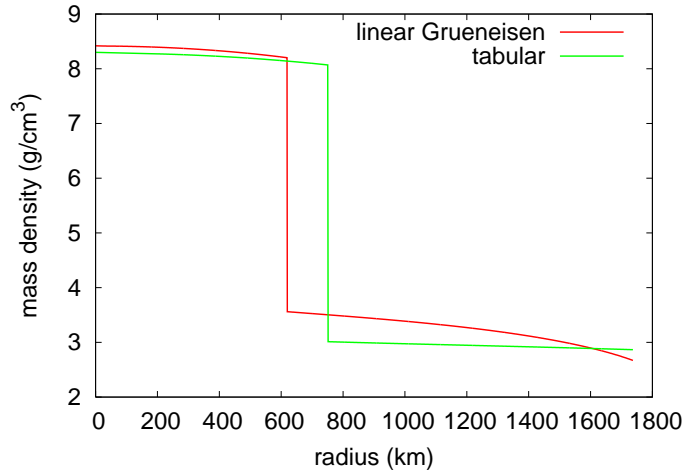


FIG. 12: Radial density distribution in the Moon calculated using different equations of state.

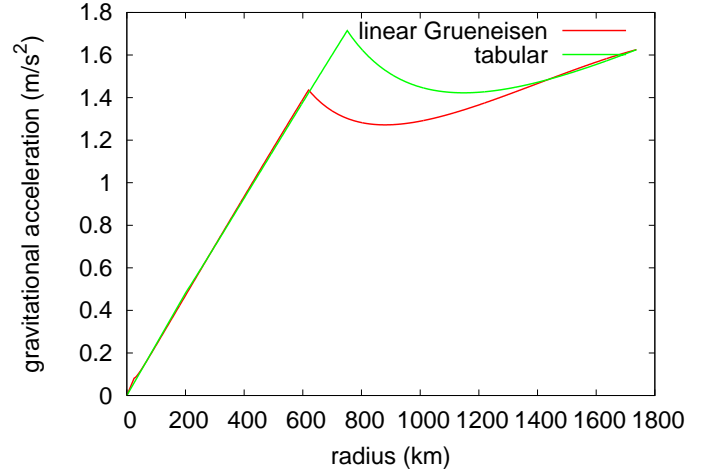


FIG. 13: Radial gravity distribution in the Moon calculated using different equations of state.



### E. Mars

For Mars, the EOS gave similar pressure distributions in the mantle, and deviated greatly in the core. The core radii differed significantly. The density distributions were significantly different, but mostly because of the difference in core radius. The core pressures were all above the  $\alpha$ - $\epsilon$  phase transition. The gravitational acceleration from each EOS was very similar in the core, but deviated substantially where the core radii differed and in the mantle. For simulation purposes, the EOS not equivalent. (Figs 14 to 16.)

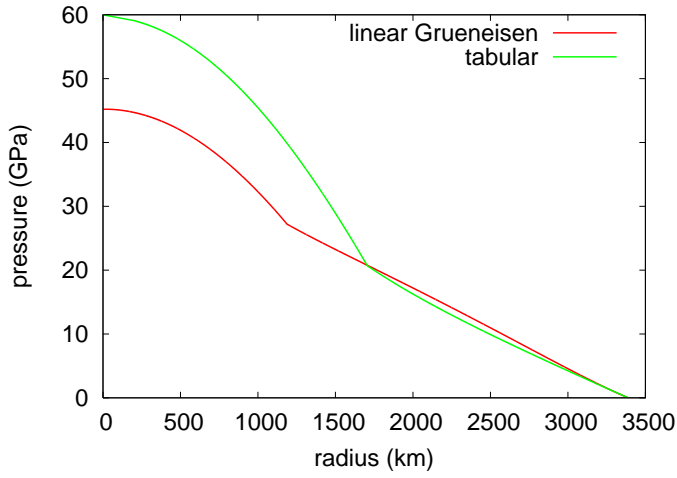


FIG. 14: Radial pressure distribution in Mars calculated using different equations of state.

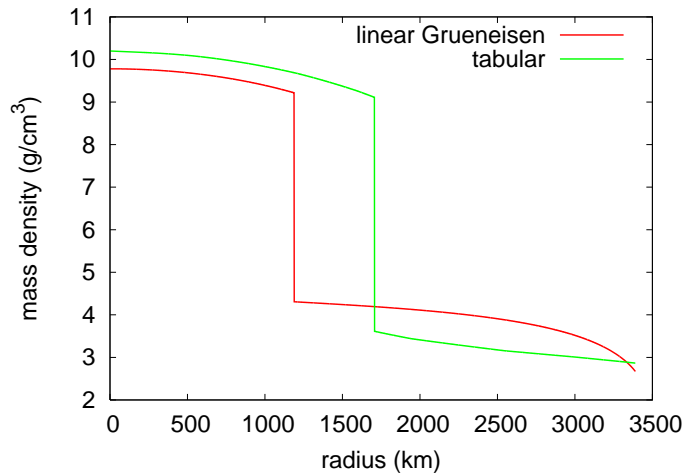


FIG. 15: Radial density distribution in Mars calculated using different equations of state.

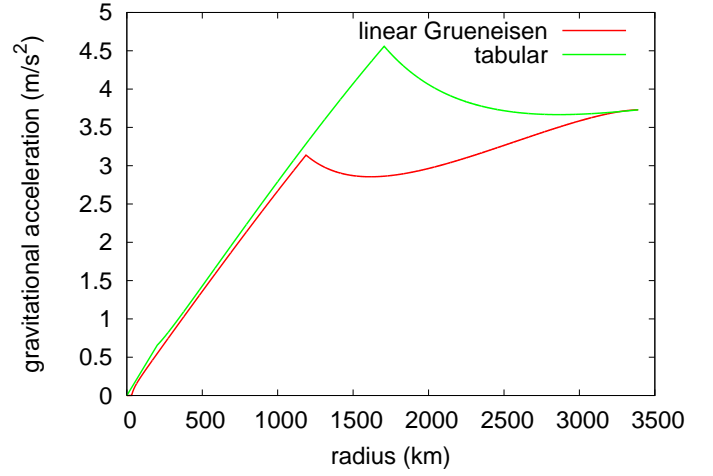


FIG. 16: Radial gravity distribution in Mars calculated using different equations of state.

## V. CONCLUSIONS

The isostatic equations were used to calculate density distributions for Mercury, Venus, Earth, the Moon, and Mars, assuming different EOS for the structural components, and optimizing the core radius to constrain the overall mass to be correct. Two pairs of EOS were considered for Fe and basalt, either linear Grüneisen fits to subsets of published shock data, or more detailed EOS constructions including phase changes and nonlinearities in the shock data. The core radius of Earth, which is by far the best known, was reproduced reasonably well using both types of EOS. The other radii, and structures for all the bodies, varied significantly between the EOS, though to a varying degree. The structures were used to calculate the moment of inertia ratio for each body, as an independent test of the accuracy of each structure.

Better overall agreement with the observed proper-

ties of the rocky bodies considered was obtained with the linear Grüneisen EOS than the more carefully constructed tabular EOS. This does not imply that the linear Grüneisen EOS are more accurate models of Fe and basalt, but that the properties of the bodies are represented more closely by the simpler EOS, presumably because the compositions deviate significantly from Fe and basalt in the core and mantle respectively. The simpler EOS do not reproduce the moment of inertia ratios perfectly, and deviate particularly for the Moon and Mars.

The linear Grüneisen EOS seem to be a reasonable starting point for simulations of large-scale impacts on these bodies, more so than the tabular EOS. These results also suggest that more detailed EOS for the postulated compositions of the bodies can be evaluated to some degree by their improvement over Fe and basalt in calculating the moment of inertia ratios.

- 
- [1] For instance, R.G. McQueen, S.P. Marsh, T.W. Taylor, J.N. Fritz, and W.J. Carter, in R. Kinslow (Ed.), “High Velocity Impact Phenomena” (Academic Press, New York, 1970).
  - [2] For instance, A. Dewaele, P. Loubeyre, F. Occelli, M. Mezouar, P.I. Dorogokupets, and M. Torrent, *Phys. Rev. Lett.* **97**, 215504 (2006).
  - [3] For instance, D.C. Swift, G.J. Ackland, A. Hauer, and G.A. Kyrala, *Phys. Rev. B* **64**, 214107 (2001).
  - [4] For instance, D.C. Swift, D.L. Paisley, K.J. McClellan, and G.J. Ackland, *Phys. Rev. B* **76**, 134111 (2007).
  - [5] D.C. Swift, A. Seifter, D.B. Holtkamp, V.W. Yuan, D. Bowman, and D.A. Clark, *Phys. Rev. B* **77**, 092102 (2008).
  - [6] H.G. Hughes, F.N. App, and T.R. McGetchin, *Proc. Conf. on Comparisons of Mercury and the Moon*, Houston, TX, 15-17 Nov. 1976 (Lunar Science Institute, 1977).
  - [7] R.A. Lyttleton, *Mon. Not. Roy. Astr. Soc.* **129**, 21 (1965).
  - [8] R.A. Lyttleton, *Astrophys. Space Sci.* **5**, 18 (1969).
  - [9] D. Gubbins and E. Herrero-Bervera, “Encyclopedia of geomagnetism and paleomagnetism” (Springer, New York, 2007).
  - [10] G.I. Kerley, *Structures of the Planets Jupiter and Saturn*, report KTS04-1 (Kerley Technical Services, Appomattox, 2004).
  - [11] S. Seager, M. Kuchner, C.A. Hier-Majumder, and B. Militzer, *ApJ* **669**, pp 1279-1297 (2007).
  - [12] O. Grasset, J. Schneider, and C. Sotin, *ApJ* **693**, pp 722-733 (2009).
  - [13] M. van Thiel, *Compendium of Shock Wave Data*, Lawrence Livermore National Laboratory report UCRL-50108 (1966).
  - [14] J.F. Barnes and S.P. Lyon, *SESAME Equation of State Number 7530, Basalt*, Los Alamos National Laboratory report LA-11253-MS (1988).
  - [15] G.I. Kerley, *Multiphase Equation of State for Iron*, Sandia National Laboratories report SAND93-0227 (1993).
  - [16] C.F. Yoder in T.J. Ahrens (Ed.), “Global Earth Physics: A Handbook of Physical Constants” (American Geophysical Union, Washington DC, 1995).